pattern cell types. TMM controls the orientation of asymmetric divisions that create the minimal one-celled stomatal spacing pattern and may also participate broadly in regulating cell proliferation and differentiation based on positional context. The latter function appears analogous to the CLV1/CLV2 signaling pathway that regulates the balance between stem cell maintenance in the central shoot apical meristem and cell differentiation at the meristem flanks (*9*). In contrast, TMM functions in cells that are dispersed within the developing epidermis and have different fate potentials, ranging from multipotent stem cells that may undergo a formative asymmetric division to meristemoids that invariably mature into stomata.

Additional support for the importance of position-dependent cell proliferation in epidermal patterning comes from the *STOMATAL DENSITY AND DISTRIBUTION 1* locus, which encodes a processing protease likely to participate in cell signaling (*1*). The control of cell division relative to nearby differentiating cells is likely to be a recurring theme in plant development.

References and Notes

1. D. Berger, T. Altmann, *Genes Dev.* **14**, 1119 (2000).
2. J. A. Nadeau, F. D. Sack, in *The* Arabidopsis *Book*, C. R. Somerville, E. M. Meyerowitz, Eds. (American Society of Plant Biologists, Rockville, MD, 2002), www.aspb.org/publications/arabidopsis
3. Supplemental materials and methods are available on *Science* Online at www.sciencemag.org/cgi/content/full/296/5573/1697/DC1.
4. M. D. Geisler, J. A. Nadeau, F. D. Sack, *Plant Cell* **12**, 2075 (2000).
5. A. V. Kajava, *J. Mol. Biol.* **277**, 519 (1998).
6. K. Nakai, M. Kanehisa, *Genomics* **14**, 897 (1992).
7. T.-L. Jinn, J. M. Stone, J. C. Walker, *Genes Dev.* **14**, 108 (2000).
8. K. U. Torii *et al.*, *Plant Cell* **8**, 735 (1996).
9. S. E. Clark, R. W. Williams, E. M. Meyerowitz, *Cell* **89**, 575 (1997).
10. J. Li, J. Chory, *Cell* **90**, 929 (1997).
11. L. Gomez-Gomez, T. Boller, *Mol. Cell* **5**, 1003 (2000).
12. G.-L. Wang, W.-H. Song, D.-L. Ruan, S. Sideris, P. C. Ronald, *Mol. Plant Microbe Interact.* **9**, 850 (1996).
13. S. Jeong, A. E. Trotochaud, S. E. Clark, *Plant Cell* **11**, 1925 (1999).
14. D. A. Jones, C. M. Thomas, K. E. Hammond-Kosack, P. J. Balint-Kurti, J. D. G. Jones, *Science* **266**, 789 (1994).
15. M. S. Dixon *et al.*, *Cell* **84**, 451 (1996).
16. A. E. Trotochaud, T. Hao, G. Wu, Z. Yang, S. E. Clark, *Plant Cell* **11**, 393 (1999).
17. M. Yang, F. D. Sack, *Plant Cell* **7**, 2227 (1995).
18. G.-L. Wang *et al.*, *Plant Cell* **10**, 765 (1998).
19. M. Geisler, M. Yang, F. D. Sack, *Planta* **205**, 522 (1998).
20. M. J. Geisler, J. A. Nadeau, F. D. Sack, unpublished data.
21. P. M. Donnelly, D. Bonetta, H. Tsukaya, R. E. Dengler, N. G. Dengler, *Dev. Biol.* **215**, 407 (1999).
22. Single-letter abbreviations for the amino acid residues are as follows: A, Ala; C, Cys; D, Asp; E, Glu; F, Phe; G, Gly; H, His; I, Ile; K, Lys; L, Leu; M, Met; N, Asn; P, Pro; Q, Gln; R, Arg; S, Ser; T, Thr; V, Val; W, Trp; and Y, Tyr.

23. We are grateful to M. Bolgar and C. Lee for technical assistance, to M. Geisler for Fig. 1A, and to B. Ding for the use of his confocal microscope. S. Cutler, D. Ehrhardt, and C. Somerville generously provided the GFP-PIP2A line. Funded by NSF grant IBN-9904826 to F.D.S and J.A.N.

7 January 2002; accepted 23 April 2002

Probing Protein Electrostatics with a Synthetic Fluorescent Amino Acid

Bruce E. Cohen,[1]† Tim B. McAnaney,[2]* Eun Sun Park,[2]* Yuh Nung Jan,[1] Steven G. Boxer,[2] Lily Yeh Jan[1]

Electrostatics affect virtually all aspects of protein structure and activity and are particularly important in proteins whose primary function is to stabilize charge. Here we introduce a fluorescent amino acid, Aladan, which can probe the electrostatic character of a protein at multiple sites. Aladan is exceptionally sensitive to the polarity of its surroundings and can be incorporated site-selectively at buried and exposed sites, in both soluble and membrane proteins. Steady-state and time-resolved fluorescence measurements of Aladan residues at different buried and exposed sites in the B1 domain of protein G suggest that its interior is polar and heterogeneous.

High-resolution structures provide the primary basis for analysis of protein function, yet investigations into other physical properties such as protein dynamics and electrostatics have been hampered by experimental limitations. For electrostatics in particular, the lack of general techniques for measuring static and dynamic electric fields within a protein has made it difficult to address even a most basic question: how polar is a protein? A protein's polarity—that is, its capacity to solvate charge—affects the strengths of all electrostatic interactions within the protein, as well as the strengths of interactions with proteins, substrates, and other ligands, making it a critical determinant of protein structure, stability, and, ultimately, activity (*1*, *2*). Ideas about the polarity of the protein interior have progressed from simple models of proteins as nonpolar and homogeneous, described by a low dielectric constant (i.e., $\varepsilon = 2$ to 4), to more complex models that consider sources of local heterogeneity. Computational models suggest that local dielectric properties can vary considerably and, in some cases, correspond to polar solvents, even in the protein interior (*1*, *3*). Examining protein solvation experimentally has usually relied on the fortuitous affinity of probes for ligand-binding sites (*4*–*9*) or the presence of endogenous long-wavelength chromophores (*10*, *11*), typically limiting such measurements to individual, sometimes ill-defined, locations within particular proteins. Tryptophan fluorescence has also been used as an intrinsic local environmental probe (*12*, *13*), but tryptophan's utility is limited by its complex photophysics. An ideal probe for studying protein dynamics and electrostatics would be sensitive to its environment and could be incorporated site-specifically throughout any protein of interest. Toward that end, we have synthesized an environment-sensitive fluorescent amino acid, Aladan, and incorporated it site-specifically into proteins by both nonsense suppression and solid-phase synthesis, and we have used it to probe the electrostatic character of the B1 domain of streptococcal protein G (GB1) at multiple sites by steady-state and time-resolved fluorescence.

The fluorophore 6-dimethylamino-2-acylnaphthalene (DAN) undergoes a large charge redistribution upon excitation and has nearly ideal environment sensor properties (*4*, *5*, *12*, *14*). As shown in Fig. 1, an alanine derivative of DAN (Aladan, compound 3) (*15*) was synthesized and either converted to its Fmoc derivative (compound 4) for solid-phase peptide synthesis or functionalized (compound 5) for coupling to a *T. thermophila* suppressor tRNA (*16*) for nonsense suppression. The bisamide *N*-acetyl-Aladanamide (NAAA, Fig. 1B, inset) mimics Aladan within a peptide and exhibits a similar solvatochromism as observed for other DAN probes (*12*, *14*), including a large shift in emission maximum (λ_{max}) that depends on solvent polarity (from 409 nm in heptane to 542 nm in water), as well as emission at longer wavelengths in hydroxylated solvents relative to those of aprotic solvents of comparable polarities (Fig. 1, B and C). Other spectral characteristics such as absorption show much less dramatic changes (*17*). The λ_{max} of NAAA in water is not sensitive to changes in pH be-

[1]Howard Hughes Medical Institute and Departments of Physiology and Biochemistry, University of California San Francisco, San Francisco, CA 94143, USA. [2]Department of Chemistry, Stanford University, Stanford, CA 94305, USA.

*These authors contributed equally to this work.
†To whom correspondence should be addressed. Email: bcohen@itsa.ucsf.edu

tween 3 and 12 or to changes in salt concentration (Fig. 1C).

A variety of techniques have been used to introduce synthetic probes into proteins, including the site-specific incorporation of unnatural amino acids (*18*–*21*). We used nonsense suppression methodology (*16*, *20*) to insert Aladan at various sites in the Kir2.1 and *Shaker* potassium channels as examples of whether proteins with Aladan substitutions could fold and function properly. *Xenopus* oocytes coinjected with Aladan-charged suppressor tRNA (*15*) and channel cRNA containing nonsense mutations showed typical Kir or *Shaker* currents (fig. S1), with good suppression for residues in all protein environments (i.e., aqueous, lipid, and buried). Suppression at Kir2.1 Trp^{96} (fig. S1A) is notable in that this position should be particularly sensitive to mutation, as it is completely conserved in the Kir family and is predicted to lie buried within three transmembrane helices (*22*). These experiments show that Aladan is compatible with the cellular biosynthetic machinery, a property of unnatural amino acids that has been impossible to predict with any certainty (*20*), and that the Aladan side chain is not inherently disruptive, even when buried within the protein.

As a dielectric-sensitive fluorophore that can occupy buried sites, Aladan provides a means to examine the physical properties of the protein core. We incorporated Aladan by solid-phase synthesis at four different sites in GB1, a highly thermostable IgG-binding domain that has been characterized extensively in structure, folding, and engineering studies (*23*–*27*). Proteins with Aladan substitutions at exposed (Ala^{24}), partially exposed (Trp^{43}), and buried (Leu^{7} and Phe^{30}) residues each show a distinct fluorescence spectrum (Fig. 2, A and B). All fluorescent proteins retain the same tertiary fold as wild-type GB1, judging from affinity for ligand (*17*), accessibility of Aladan side chains to the collisional quencher iodide (fig. S2A), chemical denaturation (fig. S2B), and proton NMR (fig. S2, C and D). Interestingly, the λ_{max} of the exposed Aladan at Ala^{24} is shifted 15 nm toward the blue end of the spectrum compared with NAAA in buffer, which may reflect the partial shielding of surface side chains or dielectric differences between bulk water and the protein's hydration shell. The λ_{max} values of Aladan at the two buried sites differ by >10 nm, although both native residues are part of the inner core of the protein and have <5% exposed surface area (*23*). Comparing these λ_{max} values to those in solvent, the fluorophore at Phe^{30} falls closest to ethyl acetate ($\varepsilon = 6$) and the one at Leu^{7} closest to acetone ($\varepsilon = 21$). Previous steady-state measurements using noncovalently attached probes at putative interior ligand-binding sites have similarly found proteins in solution to behave like polar solvents (*4*, *8*). Some computational models have attributed large calculated macroscopic dielectric constants to the mobile polar groups on the surface of the protein (*3*, *28*), whereas models of local internal dielectric constants that explicitly represent solvent have found polar character in the core (*29*), consistent with the fluorescence data presented here.

However, steady-state comparisons to bulk solvent may underestimate protein polarity, as dielectric relaxation occurs on femto- to picosecond time scales in nonviscous solvents (*30*), making it essentially instantaneous relative to the fluorescence lifetime [$\tau = 3.4$ ns for compound 1 in dimethyl sulfoxide (DMSO)]. Within proteins, dielectric relaxation can be more complex, as the local reorganization of polar groups may be restricted (*5*, *6*). Depending on the relative rates of protein relaxation and fluorophore emission, the steady-state fluorescence spectrum may not directly reflect the dielectric response.

We therefore measured the time depen-

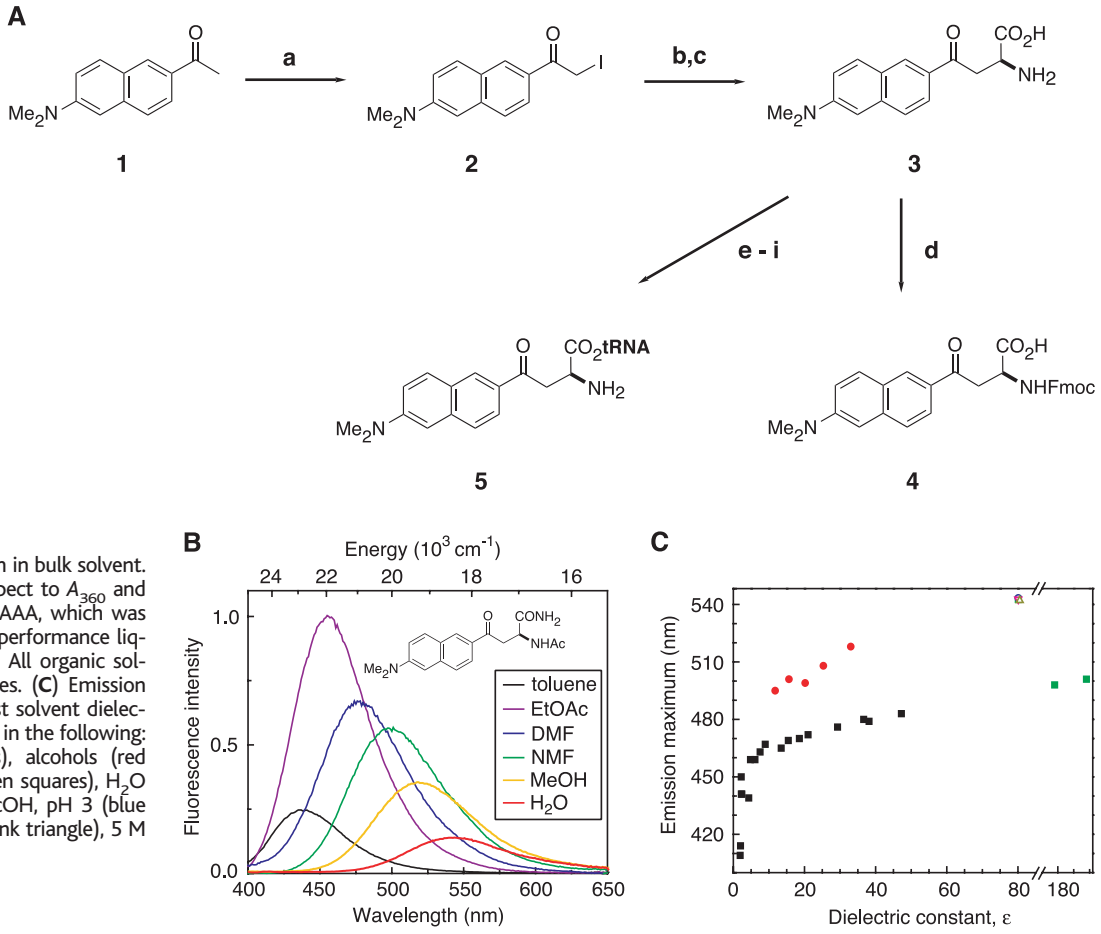

Fig. 1. Synthesis and fluorescence of Aladan. (**A**) Synthesis of Aladan derivatives from acedan (*14*). Reagents: (a), $LiN(SiMe_3)_2$ in tetrahydrofuran (THF), −78°C, then I_2; (b), $Ph_2CNCH_2CO_2{}^tBu$, cinchonidinium catalyst, $CsOH{\cdot}H_2O$, CH_2Cl_2, –70°C; (c), trifluoroacetic acid (TFA), $HSCH_2CH_2SH$; (d), Fmoc succinimidyl ester, *N*,*N*′-dimethylformamide (DMF); (e), allylchloroformate, $NaHCO_3$, THF/H_2O; (f), $ClCH_2CN$, Et_3N, DMF; (g), pdCpA, DMF; (h), AcOH, *N*-methylmorpholine, DMF, then $Pd(Ph_3P)_4$; (i), *T. thermophila* suppressor tRNA with T4 RNA ligase and reagents, as described (*16*, *20*), 37°C, 8 min. (**B**) Structure and steady-state emission spectra of NAAA after 360-nm excitation in bulk solvent. Spectra are normalized with respect to A_{360} and were measured with 200 nM NAAA, which was purified by reversed-phase high performance liquid chromatography before use. All organic solvents were dried over 3 Å sieves. (**C**) Emission maxima of NAAA plotted against solvent dielectric constant [ε values from (*33*)] in the following: aprotic solvents (black squares), alcohols (red circles), protic amides (solid green squares), H_2O (open green square), 10 mM AcOH, pH 3 (blue circle), 10 mM NaOH, pH 12 (pink triangle), 5 M GuHCl (green triangle).

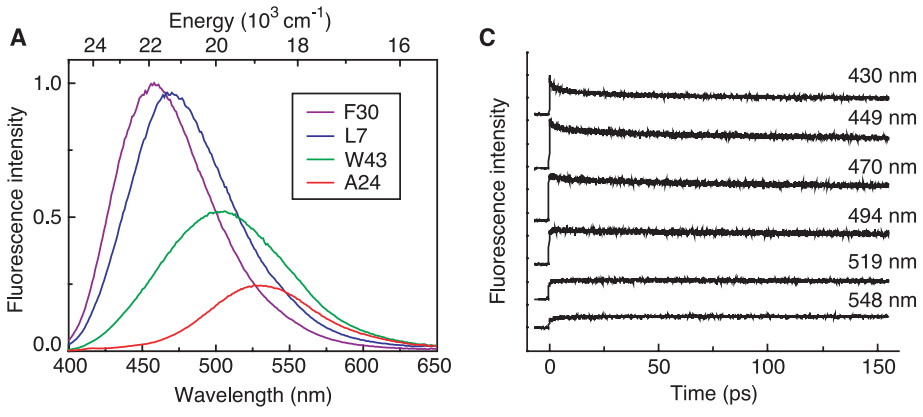

Fig. 2. Steady-state and time-resolved fluorescence of GB1 Aladan mutants. (**A**) Steady-state emission spectra of Phe^{30}, Leu^{7}, Trp^{43}, and Ala^{24} mutants after 360-nm excitation. Spectra are normalized with respect to A_{360}. Solutions contained 200 nM protein in 150 mM NaCl and 50 mM NaOAc, pH 5.4. (**B**) Visible differences in emission between buried (Phe^{30}), partially exposed (Trp^{43}), and exposed (Ala^{24}) Aladan residues, in 500 nM GB1 solutions illuminated with a hand-held 354-nm power source. (**C**) Fluorescence upconversion signal of the Phe^{30} GB1 mutant, excited at 400 nm and probed at emission energies (top to bottom) from 23,256 cm^{-1} (430 nm) to 18,256 cm^{-1} (548 nm), in 1000 cm^{-1} decrements.

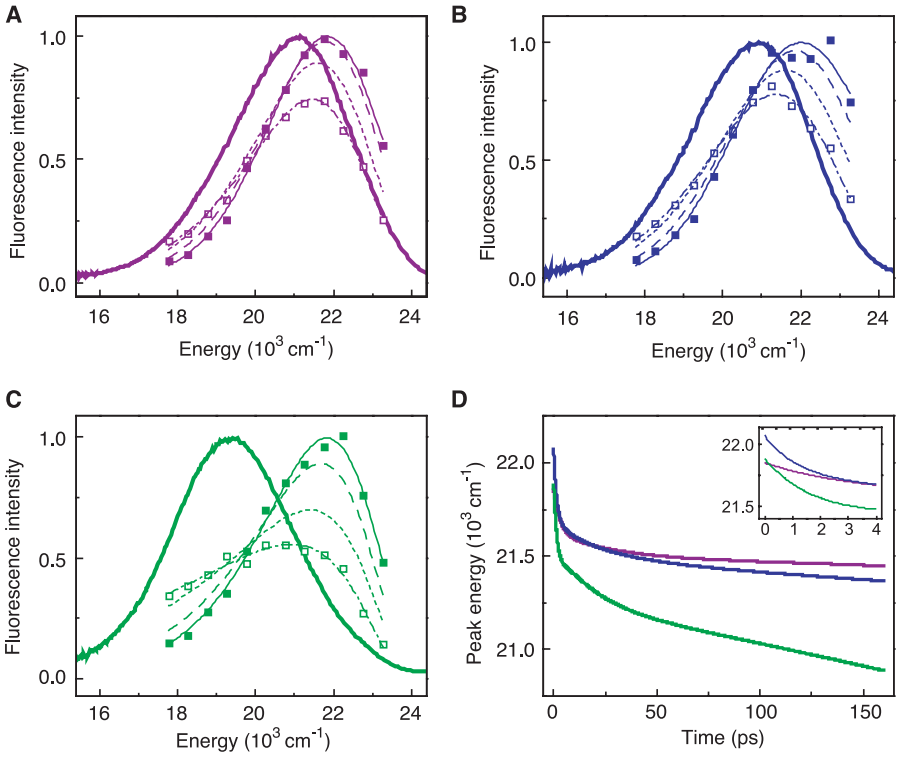

Fig. 3. Spectral reconstruction and dynamic Stokes shifts of GB1 Aladan mutants. (**A**) Reconstructed emission spectra of the Phe^{30} mutant at 200 fs (solid line), 1 ps (dashed), 10 ps (dotted), and 150 ps (dot dashed) with data points for 200 fs (solid squares) and 150 ps (open squares). Other data points are omitted for clarity. Thick line is steady-state emission. (**B**) Reconstructed spectra of the Leu^{7} mutant. (**C**) Reconstructed spectra of the Trp^{43} mutant. (**D**) Dynamic Stokes shifts as characterized by the time dependence of peak emission energies of the Phe^{30} (purple), Leu^{7} (blue), and Trp^{43} (green) mutants. Inset shows detail of the first 4 ps.

dence of the Aladan emission spectrum at one surface (Trp^{43}) and two buried (Leu^{7} and Phe^{30}) sites by fluorescence upconversion (*31*, *32*), a gating technique capable of femtosecond time resolution. For all proteins, the emission measured at shorter wavelengths exhibits a rapid decay and at longer wavelengths exhibits a rise, evidence of relaxation from high- to low-energy emitting conformations (Fig. 2C and fig. S3, A and B). Reconstructed emission spectra (Fig. 3, A to C) show that the probe emission starts from essentially the same energy in all proteins and then redshifts due to solvation. This dynamic Stokes shift (Fig. 3D) reveals comparable solvation responses in the first few picoseconds for all three sites, with Aladan at the surface site then undergoing a larger decrease in emission energy than at the buried sites, which show similar behavior. For all mutants, the emission reaches 40 to 60% of the steady-state value over the first 160 ps; in comparison, DMSO relaxation around the free fluorophore, compound 1, is >90% complete at this point (*17*). Time-resolved anisotropy of the surface fluorophore indicates no significant reorientation on this time scale, excluding movement of the probe itself as the source of solvation (fig. S4). The solvation differences between the surface and buried probes are consistent with the steady-state data (Fig. 2A) and suggest that Aladan steady-state emission reflects the local dielectric response.

Picosecond relaxation has been observed at individual sites in other proteins and has been characterized as the inertial solvation response of either the surrounding bulk water (*6*, *13*) or the protein (*9*, *11*). In this study, the initial ultrafast responses lead to comparable energy decreases for either buried or surface residues, raising the interesting possibilities that significant local inertial responses can occur throughout the protein, or that ultrafast aqueous solvation exerts similar effects over all regions of the protein. Significant fractions of these solvation responses occur within the time frame of the fastest measured physiological processes and appear to occur throughout the protein. This suggests the importance of dynamic elements in models of protein solvation, particularly for charge-stabilizing proteins, such as ion channels and electron transfer proteins, which may have evolved specific dynamic solvation mechanisms.

Aladan offers certain advantages over other probes for characterizing these dynamics, including its keen environmental sensitivity and its ability to label proteins site-specifically at buried, transmembrane, or interface positions, even in complex membrane proteins. Observed differences between intrinsic and covalently tethered fluorophores (*13*) demonstrate that attaching a probe to a protein via a side chain–reactive linker creates uncertainty in where the probe sits relative to the protein. With Aladan,

the probe is held a single methylene from the backbone and can reasonably be assumed to adopt configurations similar to those of other large side chains within the structural contexts. This permits a spatial resolution important for understanding the physiological functions of proteins.

References and Notes

1. A. Warshel, S. T. Russell, *Q. Rev. Biophys.* **17**, 283 (1984).
2. C. N. Schutz, A. Warshel, *Proteins* **44**, 400 (2001).
3. J. W. Pitera, M. Falta, W. F. van Gunsteren, *Biophys. J.* **80**, 2546 (2001).
4. R. B. Macgregor, G. Weber, *Nature* **319**, 70 (1986).
5. D. W. Pierce, S. G. Boxer, *J. Phys. Chem.* **96**, 5560 (1992).
6. X. J. Jordanides, M. J. Lang, X. Y. Song, G. R. Fleming, *J. Phys. Chem. B* **103**, 7995 (1999).
7. E. S. Park, S. S. Andrews, R. B. Hu, S. G. Boxer, *J. Phys. Chem. B* **103**, 9813 (1999).
8. E. L. Mertz, L. I. Krishtalik, *Proc. Natl. Acad. Sci. U.S.A.* **97**, 2081 (2000).
9. P. Changenet-Barret, C. T. Choma, E. F. Gooding, W. F. DeGrado, R. M. Hochstrasser, *J. Phys. Chem. B* **104**, 9322 (2000).
10. M. A. Steffen, K. Lao, S. G. Boxer, *Science* **264**, 810 (1994).
11. R. R. Riter, M. D. Edington, W. F. Beck, *J. Phys. Chem.* **100**, 14198 (1996).
12. J. R. Lakowicz, *Principles of Fluorescence Spectroscopy* (Kluwer Academic/Plenum, New York, ed. 2, 1999).
13. S. K. Pal, J. Peon, A. H. Zewail, *Proc. Natl. Acad. Sci. U.S.A.* **99**, 1763 (2002).
14. G. Weber, F. J. Farris, *Biochemistry* **18**, 3075 (1979).
15. Supplementary materials and methods are available on *Science* Online.
16. M. W. Nowak *et al.*, *Methods Enzymol.* **293**, 504 (1998).
17. B. E. Cohen *et al.*, unpublished data.
18. L. Wang, A. Brock, B. Herberich, P. G. Schultz, *Science* **292**, 498 (2001).
19. T. W. Muir, D. Sondhi, P. A. Cole, *Proc. Natl. Acad. Sci. U.S.A.* **95**, 6705 (1998).
20. V. W. Cornish *et al.*, *Proc. Natl. Acad. Sci. U.S.A.* **91**, 2910 (1994).
21. G. Turcatti *et al.*, *J. Biol. Chem.* **271**, 19991 (1996).
22. D. L. Minor Jr., S. J. Masseling, Y. N. Jan, L. Y. Jan, *Cell* **96**, 879 (1999).
23. A. M. Gronenborn *et al.*, *Science* **253**, 657 (1991).
24. D. L. Minor Jr., P. S. Kim, *Nature* **371**, 264 (1994).
25. S. M. Malakauskas, S. L. Mayo, *Nature Struct. Biol.* **5**, 470 (1998).
26. S. Nauli, B. Kuhlman, D. Baker, *Nature Struct. Biol.* **8**, 602 (2001).
27. N. Kobayashi, S. Honda, H. Yoshii, E. Munekata, *Biochemistry* **39**, 6564 (2000).
28. T. Simonson, C. L. Brooks III, *J. Am. Chem. Soc.* **118**, 8452 (1996).
29. G. King, F. S. Lee, A. Warshel, *J. Chem. Phys.* **95**, 4366 (1991).
30. E. W. Castner Jr., M. Maroncelli, *J. Mol. Liq.* **77**, 1 (1998).
31. R. J. Stanley, S. G. Boxer, *J. Phys. Chem.* **99**, 859 (1995).
32. M. L. Horng, J. Gardecki, A. Papazyan, M. Maroncelli, *J. Phys. Chem.* **99**, 17311 (1995).
33. C. Wohlfarth, *Static Dielectric Constants of Pure Liquids and Binary Liquid Mixtures* (Springer-Verlag, Berlin and New York, 1991).

34. We are grateful to W. Lim and J. Weissman for advice and generous time on their fluorimeter; C. Turck for peptide synthesis and use of his mass spectrometer; V. Basus for help with NMR; D. Agard for advice and use of his CD; A. Ting for advice about nonsense suppression; M. Yu and L. Ackerman for technical assistance; and D. Minor and members of the Jan and Boxer labs for ideas and encouragement. The fluorescence upconversion setup used for this work is located at the Stanford FEL Center supported by Air Force Office of Scientific Research grant F49620-00-1-0349. This study was supported by grants from the NIH (GM27738 to S.G.B. and MH65334 to L.Y.J.). L.Y.J. and Y.N.J. are HHMI Investigators.

Supporting Online Material

www.sciencemag.org/cgi/content/full/VOL/296/5573/1700/DC1
Methods
Figs. S1 to S4

26 December 2001; accepted 19 April 2002

A Natural Product That Lowers Cholesterol As an Antagonist Ligand for FXR

Nancy L. Urizar,[1] Amy B. Liverman,[2] D'Nette T. Dodds,[1] Frank Valentin Silva,[1] Peter Ordentlich,[3] Yingzhuo Yan,[3] Frank J. Gonzalez,[4] Richard A. Heyman,[3] David J. Mangelsdorf,[2] David D. Moore[1]*

Extracts of the resin of the guggul tree (*Commiphora mukul*) lower LDL (low-density lipoprotein) cholesterol levels in humans. The plant sterol guggulsterone [4,17(20)-pregnadiene-3,16-dione] is the active agent in this extract. We show that guggulsterone is a highly efficacious antagonist of the farnesoid X receptor (FXR), a nuclear hormone receptor that is activated by bile acids. Guggulsterone treatment decreases hepatic cholesterol in wild-type mice fed a high-cholesterol diet but is not effective in FXR-null mice. Thus, we propose that inhibition of FXR activation is the basis for the cholesterol-lowering activity of guggulsterone. Other natural products with specific biologic effects may modulate the activity of FXR or other relatively promiscuous nuclear hormone receptors.

Cholesterol metabolism is tightly regulated at multiple levels, including its release in the form of bile acids. A negative feedback loop that decreases the rate of bile acid production by the liver when bile acid levels are high is an important component of this regulation. The bile acid receptor FXR (*1*–*3*) (NR1H4) mediates this and a number of other bile acid–dependent regulatory processes (*4*), establishing its central role in cholesterol metabolism. FXR is a promiscuous nuclear hormone receptor that can be activated by a number of other compounds not structurally related to bile acids (*5*–*8*). On the basis of this apparent flexibility, we hypothesized that at least a subset of compounds reported to affect cholesterol metabolism via unknown mechanisms could act by modulating FXR activity.

The gum resin of *Commiphora mukul* (guggulu in Sanskrit) has been used in Ayurvedic medicine since at least 600 BC to treat a wide variety of ailments, including obesity and lipid disorders (*9*, *10*). An ethyl acetate extract of this resin has been found to lower LDL cholesterol and triglyceride levels in humans (*11*, *12*). Since receiving regulatory approval in India in 1987, this extract, termed gugulipid, has been widely and effectively used to treat hyperlipidemia (*9*, *10*). Among a number of compounds present in this extract, the stereoisomers E- and Z-guggulsterone (*cis*- and *trans*-4,17(20)-pregnadiene-3,16-dione, respectively) (Fig. 1A) have been shown directly to decrease hepatic cholesterol levels in rodent models (*13*).

The effect of this plant product on FXR activity was initially assessed using transient transfections with a synthetic FXR responsive reporter plasmid (*14*). Z-guggulsterone alone had no effect on FXR activity, but it strongly inhibited FXR activation by chenodeoxycholic acid (CDCA), the most potent of the bile acid agonist ligands (Fig. 1B). Essentially identical results were obtained with E-guggulsterone, but the Z isomer was used for the studies described here. The inhibition of CDCA activation was dose dependent and efficacious. In the presence of 100 μM CDCA, a concentration approximately threefold above that required for half-maximal activation of FXR, 10 μM guggulsterone decreased FXR transactivation by nearly 50%

[1]Department of Molecular and Cellular Biology, Baylor College of Medicine, 1 Baylor Plaza, Houston, TX 77030, USA. [2]Howard Hughes Medical Institute, University of Texas - Southwestern Medical Center, 5323 Harry Hines Boulevard, Dallas, TX 75390, USA. [3]X-Ceptor Therapeutics, Inc., 4757 Nexus Center Drive, San Diego, CA 92121, USA. [4]Laboratory of Metabolism, Center for Cancer Research, National Cancer Institute, Building 37, Room 3E24, Bethesda, MD 20892, USA.

*To whom correspondence should be addressed. E-mail: moore@bcm.tmc.edu